Original Article

Discrepancies in PD-L1 expression, lymphocyte infiltration, and tumor mutational burden in non-small cell lung cancer and matched brain metastases

Yanhui Zhang[1], Runfen Cheng[1], Tingting Ding[1], Jianghua Wu[1,2]^

[1]Department of Pathology, Tianjin Medical University Cancer Institute and Hospital, National Clinical Research Center for Cancer, Tianjin's Clinical Research Center for Cancer, Key Laboratory of Cancer Prevention and Therapy, Tianjin, China; [2]Department of Pathology, School of Basic Medical Sciences, Peking University Third Hospital, Peking University Health Science Center, Beijing, China

Contributions: (I) Conception and design: Y Zhang, J Wu; (II) Administrative support: J Wu; (III) Provision of study materials or patients: Y Zhang, R Cheng; (IV) Collection and assembly of data: R Cheng, T Ding; (V) Data analysis and interpretation: Y Zhang, J Wu; (VI) Manuscript writing: All authors; (VII) Final approval of manuscript: All authors.

Correspondence to: Jianghua Wu, PhD. Department of Pathology, Tianjin Medical University Cancer Institute and Hospital, National Clinical Research Center for Cancer, Tianjin's Clinical Research Center for Cancer, Key Laboratory of Cancer Prevention and Therapy, Tianjin, China; Department of Pathology, School of Basic Medical Sciences, Peking University Third Hospital, Peking University Health Science Center, 38 Xueyuan Road, Haidian District, Beijing 100191, China. Email: fjctwjh@126.com.

Background: Differences in the immune microenvironment and responses to immunotherapy may exist between primary non-small cell lung cancer (NSCLC) and brain metastases (BMs). This study aimed to investigate discrepancies in programmed death-ligand 1 (PD-L1) expression, tumor-infiltrating lymphocytes (TILs), tertiary lymphoid structures (TLS), and tumor mutational burden (TMB) between matched BMs and primary tumors (PTs) in NSCLC.

Methods: Twenty-six pairs of surgically resected BMs and corresponding PTs from NSCLC patients were collected. PD-L1 expression and TILs, including CD8, CD3, CD4, CD20, CD68, and CD21, were analyzed using immunohistochemistry (IHC) and quantitatively assessed through digital image analysis. Whole-exome sequencing (WES) was performed to investigate genomic discrepancies and variations in TMB.

Results: The density of PD-L1$^+$ cells did not differ significantly between matched PTs and BMs (P>0.99). However, BMs exhibited a higher tumor proportion score (TPS) compared to PTs (mean TPS: 31.92% *vs.* 25.96%, P=0.049), with moderate agreement in categorized TPS (κ=0.653). Analysis of TILs revealed a significant reduction in CD3$^+$ T cells (P<0.001), CD8$^+$ cytotoxic T cells (P<0.001), CD20$^+$ B cells (P<0.001), and CD68$^+$ macrophages (P=0.02) in BMs compared to PTs. BMs also exhibited a loss of TLS, with no presence of mature TLS marked by CD21 expression. The number of non-synonymous mutations was generally higher in BMs than in PTs, with only 34.69% of mutations shared between paired PTs and BMs. TMB was slightly increased in BMs (mean TMB: 34.2 mutations/Mb in BMs *vs.* 26.8 mutations/Mb in PTs; P=0.30). Additionally, the log-rank test indicated that a higher density of CD20$^+$ B cells in BMs was significantly associated with better overall survival (P=0.007).

Conclusions: Compared to primary NSCLC tumors, matched BMs show an increase in TPS of PD-L1 expression and TMB, but a significant reduction in TILs and loss of mature TLS, suggesting an immune-suppressive microenvironment in BMs. The infiltration of CD20$^+$ B cells may serve as a potential prognostic biomarker in NSCLC with BMs.

Keywords: Non-small cell lung cancer (NSCLC); brain metastases (BMs); programmed death-ligand 1 (PD-L1); tumor-infiltrating lymphocytes (TILs); tumor mutational burden (TMB)

^ ORCID: 0000-0001-7351-8933.

Submitted Aug 23, 2024. Accepted for publication Dec 11, 2024. Published online Dec 27, 2024.
doi: 10.21037/tlcr-24-735
View this article at: https://dx.doi.org/10.21037/tlcr-24-735

Introduction

The application of immune checkpoint inhibitors (ICIs) targeting programmed death receptor-1 (PD-1) and programmed death-ligand 1 (PD-L1) has led to significant advancements in the treatment of advanced non-small cell lung cancer (NSCLC), providing notable benefits to patients. Despite these advances, brain metastases (BMs) remain a major cause of cancer-related mortality in NSCLC, with brain-specific overall response rates being lower than those for lung lesions (1). Additionally, there is a lack of biomarkers that can predict responses to immunotherapy specifically for BMs in NSCLC.

In NSCLC immunotherapy, widely established biomarkers include PD-L1, tumor-infiltrating lymphocytes (TILs), tertiary lymphoid structures (TLS), and tumor mutational burden (TMB). PD-L1 expression is commonly utilized in clinical practice to identify NSCLC patients likely to benefit from ICI therapy; however, variability in PD-L1 expression between metastases and primary tumors (PTs) has been reported (2-4). TILs are crucial components of the tumor immunophenotype and significantly influence the efficacy of immunotherapy in NSCLC, but their evaluation through visual pathology is challenging (5). TLS, also known as ectopic lymphoid tissues, are lymph node-like formations that develop in non-lymphoid tissues affected by tumors, autoimmune diseases, or infections. Increasing evidence indicates that TLS presence is strongly associated with a favorable prognosis in various cancers, including NSCLC (6). The anti-tumor immune response is also influenced by the evolving tumor microenvironment, which is closely related to the activation of tumor immunogenicity during metastasis (7). TMB, defined as the number of somatic mutations in the tumor genome, is calculated as the total number of non-synonymous mutations per megabase (Mb) of the evaluated gene exon coding region in tumor tissue (8). Several clinical studies support the predictive value of TMB for immunotherapy across different cancers (9-11).

BMs may exhibit distinct immune microenvironment characteristics compared to PTs. The differences in genomic burden and immune microenvironment between PTs and BMs could contribute to the variable efficacy of immunotherapy. In this study, we analyzed PD-L1 expression, TILs, and TLS using digital image analysis and employed whole exome sequencing (WES) for genomic profiling and TMB analysis on surgically resected PTs and paired BMs. The aim was to explore discrepancies in commonly used immunotherapy-related biomarkers between PTs and their matched BMs, providing insights into the heterogeneous immunotherapeutic responses observed in NSCLC BMs. We present this article in accordance with the STROBE reporting checklist (available at https://tlcr.amegroups.com/article/view/10.21037/tlcr-24-735/rc).

Highlight box

Key findings

- Brain metastases (BMs) in non-small cell lung cancer (NSCLC) exhibit an increased tumor proportion score for programmed death-ligand 1 (PD-L1) expression and a slightly higher tumor mutational burden (TMB) compared to paired primary tumors (PTs). However, BMs also show a significant reduction in tumor-infiltrating lymphocytes (TILs) and a loss of mature tertiary lymphoid structures (TLS).

What is known and what is new?

- Discrepancies in PD-L1 expression between PTs and matched BMs have been previously reported.
- This study advances current understanding by employing digital image analysis to assess TILs and TLS. It also investigates genomic discordance and variations in TMB between PTs and matched BMs. Additionally, it highlights the prognostic importance of $CD20^+$ B cells in NSCLC with BMs.

What is the implication, and what should change now?

- The observed discrepancies in immunotherapeutic biomarkers suggest a potentially heterogeneous impact on immune responses to immunotherapy in NSCLC BMs. The immune-suppressive microenvironment in BMs underscores the importance for strategies to enhance TLS and promote TILs migration and infiltration as part of immunotherapy approaches.

Methods

Cases collection and design

This study retrospectively collected NSCLC cases with paired PTs and BMs from Department of Pathology at the

Tianjin Medical University Cancer Institute and Hospital (TMUCIH) from June 2013 to September 2021. The study was conducted in accordance with the Declaration of Helsinki (as revised in 2013) and was approved by the Ethics Committee of the TMUCIH (No. bc20241476). Written informed consent was waived due to the retrospective nature of this study. The inclusion criteria were: (I) histological confirmation of NSCLC; (II) surgical resection of both PTs and BMs; (III) tumor size ≥0.5 cm; and (IV) availability of clinical information and follow-up data. A total of 26 NSCLC cases were selected, resulting in 52 matched formalin-fixed paraffin-embedded (FFPE) blocks. All cases were reviewed by two pathologists according to the fifth edition of the World Health Organization (5th WHO) classification for lung cancer. Clinicopathological characteristics, including age, sex, smoking history, histology, and treatment, were collected. The recurrence interval refers to the time from the initial operation to the discovery of metastasis. Overall survival (OS) is defined as the length of time from diagnosis until death from any cause.

Immunohistochemistry (IHC) staining

Sequential 4-μm-thick sections from NSCLC FFPE samples were prepared for IHC staining. PD-L1 staining was conducted using the PD-L1 22C3 pharmDX kit (Dako, Carpinteria, CA, USA) on the Dako Link AS-48 autostainer system, following the manufacturer's instructions. Other IHC stains were performed using an automated staining system (BenchMark ULTRA, Roche, Ventana Medical Systems, Tucson, AZ, USA), with ready-to-use primary antibodies from ZSGB-BIO (Beijing, China), including CD8 (C8/144B), CD3 (EP41), CD4 (EP204), CD20 (L26), CD68 (KP-1), and CD21 (EP64).

Interpretation of PD-L1 staining

The tumor proportion score (TPS) for PD-L1 expression in NSCLC was assessed as the percentage of viable tumor cells (TCs) exhibiting membranous staining across whole sections. This evaluation was performed independently by two specialized pathologists, with discordant cases reviewed and discussed by a third pathologist. To obtain detailed comparative data, pathologists' scores were recorded on a point scale: negative or <1% and ranging from 1% to 100% in 5% increments. TPS was categorized using the following cut-off values: negative (<1%), low expression (1% to 49%), and high expression (≥50%).

Digital analysis of TILs

Digital image analysis was conducted on IHC slides, including those stained for PD-L1 and immune cells (ICs). IHC slides were scanned using a Leica Aperio CS2 (Leica Biosystems, Buffalo Grove, IL, USA) at ×200 magnification. Pathologists annotated the tumor areas on the digital images for analysis. The positive cell detection and cell segmentation tools in QuPath software (version 0.4.0, Belfast, UK) were employed to quantify the positive cell populations and their densities on each IHC digital slide (12).

Since markers such as CD4$^+$ for T cells are not highly specific, we initially analyzed smaller regions of interest to fine-tune parameters, mainly including intensity parameters, cell parameters, intensity threshold parameters, and score compartments. Our focus was on cell size, roundness, and 3,3'-diaminobenzidine (DAB) staining. This approach ensured that the detection results accurately represented the majority of positive cells across the entire tumor area. Representative images of PD-L1 and IC staining, along with the image analysis, are illustrated in *Figure 1* and Figure S1.

Analysis of TLS

TLS were identified using both hematoxylin and eosin (H&E) and IHC staining on multiple serial paraffin sections. Sections were stained with anti-human antibodies against CD20, and CD21 to confirm the presence of TLS by visualizing B cells, and follicular dendritic cells (FDCs). TLS were considered present and counted if they were located within the tumor or within 500 μm of the tumor's invasive margin. TLS were categorized into two maturation stages, characterized by an increasing prevalence of CD21$^+$ FDCs and mature B cells: (I) early TLS, consisting of dense CD20$^+$ lymphocytic aggregates without CD21$^+$ FDCs; and (II) mature TLS, featuring follicle-like germinal centers (GCs) with dense CD20$^+$ lymphocytic aggregates and CD21$^+$ FDCs (13,14).

WES and TMB calculation

Somatic mutation detection and TMB calculation were performed using WES data in 14 paired samples. DNA was extracted from 28 tumor samples and 14 paired normal lung tissues using TIANamp Genomic DNA Kits (Qiagen,

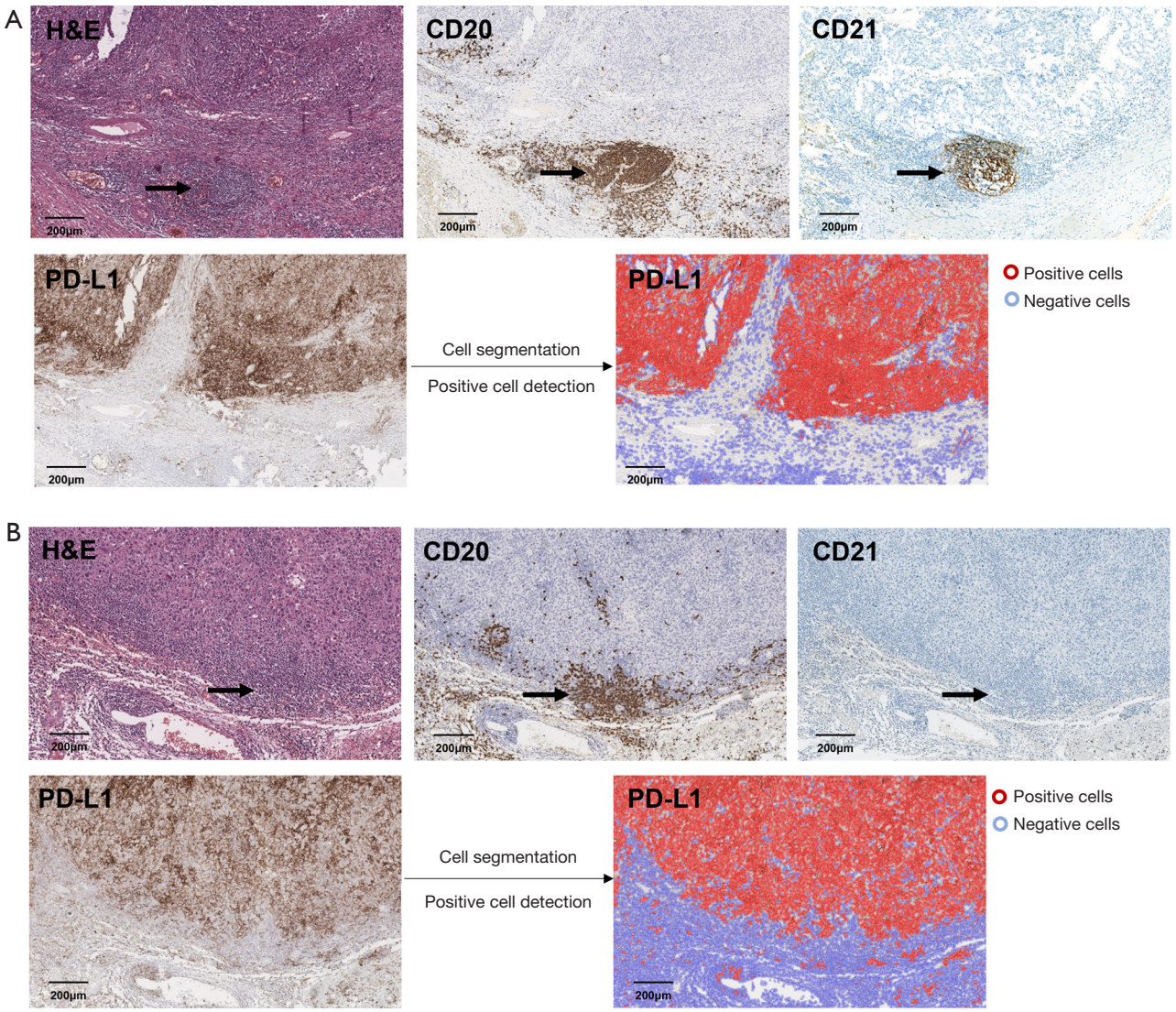

Figure 1 Summary of histological and immunohistochemical analyses in PTs and BMs of NSCLC. (A) H&E staining and IHC staining for CD20$^+$ B cells and CD21$^+$ FDCs, and digital analysis of PD-L1 positive cells in PTs. Black arrows indicate CD20$^+$ lymphocytic aggregates forming follicular-like TLS with CD21$^+$ FDCs in PTs; (B) H&E staining and IHC staining for CD20$^+$ B cells and CD21$^+$ FDCs, and digital analysis of PD-L1 positive cells in BMs of NSCLC. Black arrows indicate CD20$^+$ lymphocytic aggregates as early TLS, lacking CD21$^+$ FDCs in BMs. H&E, hematoxylin and eosin; PD-L1, programmed death-ligand 1; PTs, primary tumors; BMs, brain metastases; NSCLC, non-small cell lung cancer; IHC, immunohistochemistry; FDCs, follicular dendritic cells; TLS, tertiary lymphoid structures.

DP304-03, Hilden, Germany). Briefly, the DNA was fragmented using a hydrodynamic shearing system (Covaris, Massachusetts, USA), and DNA fragments with ligated adapter molecules at both ends were selectively enriched through polymerase chain reaction (PCR). Whole-exome libraries were constructed using the Agilent SureSelect Human All Exon V6 Kit (Agilent Technologies, Santa Clara, USA). The DNA libraries were then sequenced on the Illumina HiSeq 4000 platform (Illumina, San Diego, USA), generating sequencing reads. For library preparation and target capture, the TruePrepDNA Library Preparation Kit V2 (TD501, Vazyme, Nanjing, China) and xGen (Integrated DNA Technologies, Inc., Coralville, IA, USA) were utilized for pull-down and creation of the full exome library. The sequencing data were analyzed using standard bioinformatics pipelines to detect single nucleotide variants

Table 1 The characteristics of non-small cell lung cancer patients with brain metastases (n=26)

Parameters	Values
Age (years)	61.5 [42–71]
Sex	
Male	14 (53.8)
Female	12 (46.2)
Smoking history	
Yes	20 (76.9)
No	6 (23.1)
Histology	
Lung adenocarcinoma	21 (80.8)
Squamous cell carcinoma	5 (19.2)
Metastatic sites	
Cerebellum	14 (53.8)
Frontal lobe	6 (23.1)
Occipital lobe	6 (23.1)
Treatment	
Chemotherapy	19 (73.1)
Chemotherapy and radiotherapy	1 (3.8)
EGFR-TKI	4 (15.4)
Chemotherapy plus immunotherapy	1 (3.8)
Interval time for metastasis (months)	16.5 [2–51]
Follow-up time (months)	45 [14–92]
Overall survival	
Living	9 (34.6)
Deceased	17 (65.4)

Data are presented as median [range] or n (%). EGFR, epidermal growth factor receptor; TKI, tyrosine kinase inhibitor.

(SNVs) and insertions/deletions (indels) (15,16). TMB was calculated by counting non-synonymous mutations per Mb of coding DNA. Only protein-coding mutations were included, excluding synonymous and non-coding mutations. The TMB score was determined by dividing the total number of non-synonymous mutations by the exome size in megabases (8).

Statistical analysis

The Wilcoxon signed-rank test was applied to paired PTs and BMs to assess changes within the same patient before and after metastasis. Additionally, the Mann-Whitney test was used to provide a general evaluation of differences in cell densities between non-paired PTs and BMs. Chi-squared test was used to compared the counts of TLS between PTs and BMs. Cohen's κ coefficient was evaluated for categorized TPS, with κ values classified as poor (<0.40), moderate (0.40–0.70), or good (>0.70). The log-rank test and multivariate Cox regression analysis were used to assess the prognostic significance and hazard ratio (HR) of immune biomarkers for OS. Statistical significance was set at $P<0.05$. Analyses were conducted using SPSS Statistics version 22 (IBM Corp., Armonk, NY, USA), with figures generated using R software (version 4.0.0) and PRISM V.8 (GraphPad Software, San Diego, CA, USA).

Results

Patient characteristics

This study included 26 NSCLC patients who underwent surgical resection of BMs and had matched PTs samples. The cohort consisted of 14 males (53.8%) and 12 females (46.2%), with a median age of 61.5 years (range, 42–71 years). A history of smoking was present in 20 patients (76.9%). Histologically, 21 cases (80.8%) were classified as lung adenocarcinoma, and 5 cases (19.2%) as lung squamous cell carcinoma. The metastatic sites included the cerebellum in 14 cases (53.8%), the frontal lobe in 6 cases (23.1%), and the occipital lobe in 6 cases (23.1%). The median time to BM was 16.5 months, ranging from 2 to 51 months. Adjuvant therapy following the initial surgical resection of PTs was administered to 25 patients (96.2%). Among these, 19 patients (73.1%) received adjuvant chemotherapy, 1 patient (3.8%) received both adjuvant chemotherapy and radiotherapy, 4 patients (15.4%) were treated with epidermal growth factor receptor (EGFR)-tyrosine kinase inhibitor (TKI) targeted therapy, and 1 patient (3.8%) received a combination of adjuvant chemotherapy and immunotherapy. The follow-up duration ranged from 14 to 92 months, with a median of 45 months. During the follow-up period, 17 patients (65.4%) died from cancer. Patient characteristics for the 26 NSCLC cases with BMs are summarized in *Table 1*.

Discrepancies in PD-L1 expression between BMs and PTs

For PD-L1$^+$ cells, the Wilcoxon signed-rank test revealed no significant difference in PD-L1$^+$ cell density between

Table 2 The discrepancies of immunotherapeutic biomarkers in PTs and BMs in NSCLC

Biomarkers	PTs, mean [SD]	BMs, mean [SD]	Wilcoxon signed-rank test, P value	Mann-Whitney test, P value
TPS (%)	25.96 [30]	31.92 [30]	0.049	0.56
PD-L1 (cells/mm^2)	496.0 [313.8]	501.5 [335.9]	0.68	>0.99
CD3 (cells/mm^2)	1,007.5 [417.2]	698.8 [400.6]	<0.001	0.003
CD8 (cells/mm^2)	696.5 [415.3]	406.2 [245.9]	<0.001	0.002
CD4 (cells/mm^2)	399.6 [235.1]	307.8 [180.0]	0.10	0.15
CD20 (cells/mm^2)	284.7 [190.7]	163.3 [120.1]	<0.001	0.02
CD68 (cells/mm^2)	623.1 [266.0]	519.4 [350.9]	0.02	0.052
TMB (/Mb)	26.8 [26.5]	34.2 [28.6]	0.30	0.45

PTs, primary tumors; BMs, brain metastases; NSCLC, non-small cell lung cancer; SD, standard deviation; TPS, tumor proportion score; PD-L1, programmed death-ligand 1; TMB, tumor mutational burden.

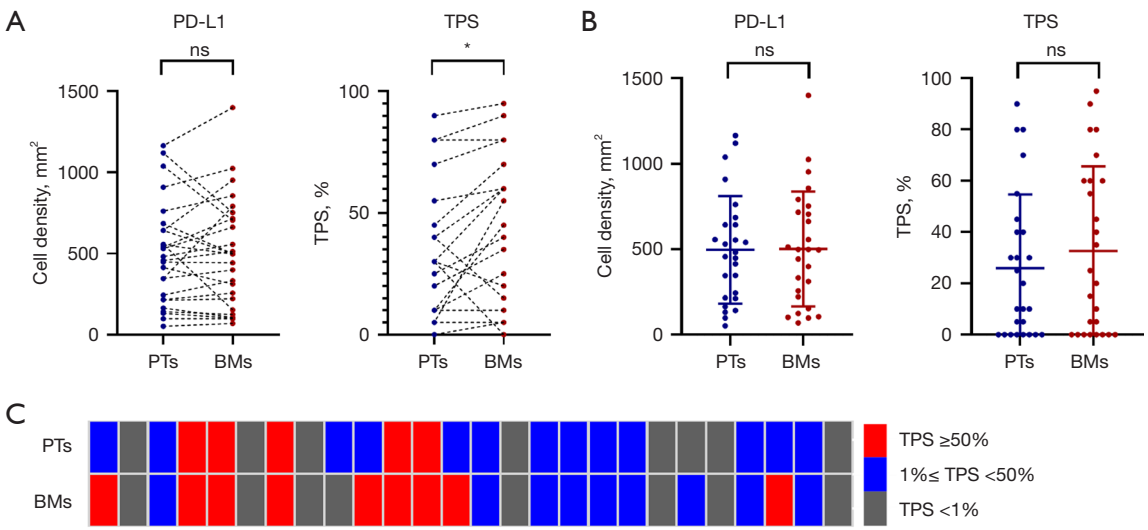

Figure 2 Comparison of PD-L1$^+$ cell density and TPS in NSCLC PTs and BMs. (A) Changes in PD-L1$^+$ cell density and TPS between paired PTs and BMs, analyzed using the Wilcoxon signed-rank test; (B) differences in PD-L1$^+$ cell density and TPS between unpaired PTs and BMs, analyzed using the Mann-Whitney *U* test; (C) heatmap categorizing TPS at cutoff values of 1% and 50% in PTs and BMs. An asterisk (*) indicates a P<0.05, while "ns" denotes no significant difference (P>0.05). PD-L1, programmed death-ligand 1; TPS, tumor proportion score; PTs, primary tumors; BMs, brain metastases; NSCLC, non-small cell lung cancer.

paired BMs and PTs (mean density: 501.5 cells/mm^2 in BMs *vs.* 496.0 cells/mm^2 in PTs, P=0.68). Similarly, the Mann-Whitney test indicated no significant difference in cell density between unpaired BMs and PTs (P>0.99). Regarding the TPS, the mean TPS was 25.96% for PTs and 31.92% for BMs. The paired analysis of TPS indicated significant heterogeneity between BMs and PTs (P=0.049), with TPS increasing in 13 BMs (50%), decreasing in 3 (11.54%), and remaining stable in 10 (38.46%) compared to matched PTs. An additional unpaired analysis showed a slightly higher TPS in BMs compared to PTs, although this difference was not statistically significant (P=0.56) (*Table 2* and *Figure 2A*,*2B*).

Using TPS cut-offs of 1% and 50%, TPS grading remained consistent in 20 paired samples (76.92%). It was upgraded in one sample (3.85%) from negative (TPS <1%) to low expression (TPS 1% to 49%) and in 4 samples (15.38%) from low expression to high expression (TPS ≥50%). Only one sample (3.85%) was downgraded from low

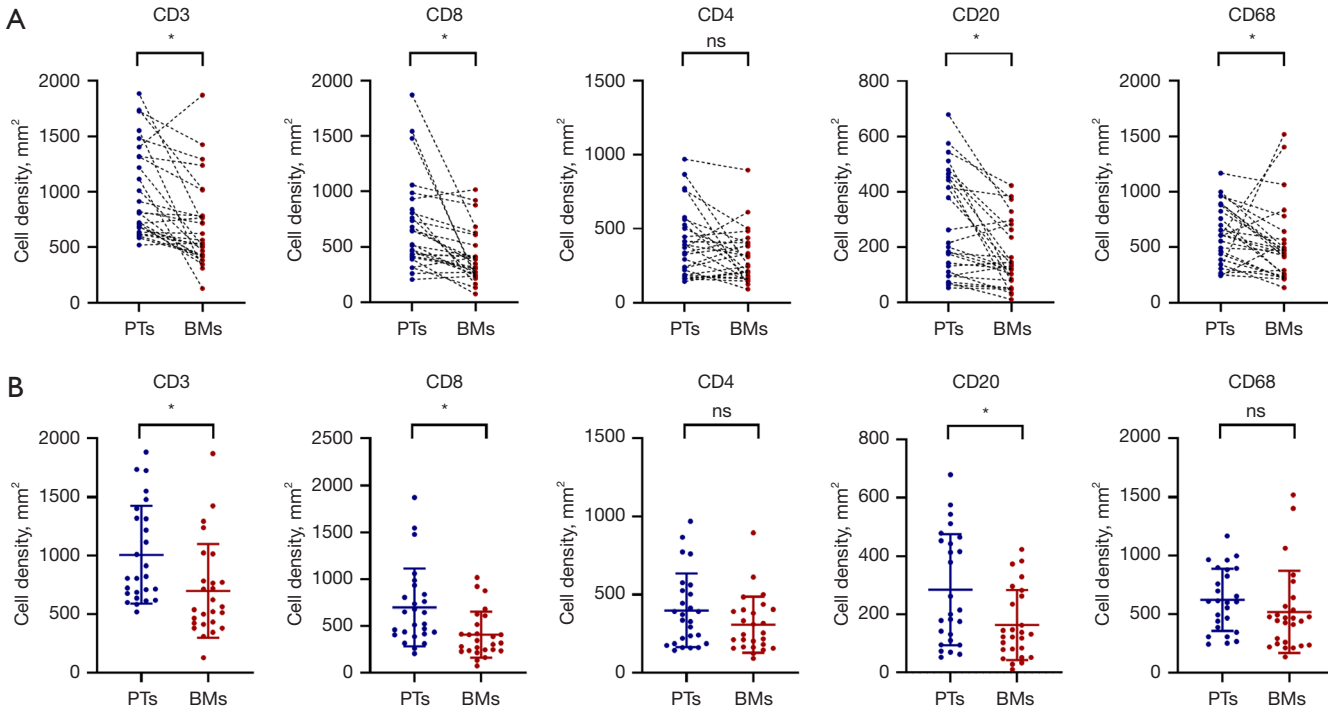

Figure 3 Comparison of immune cell density in NSCLC PTs and BMs. (A) Changes in immune cell density between paired PTs and BMs, analyzed using the Wilcoxon signed-rank test; (B) differences in immune cell density between unpaired PTs and BMs, analyzed using the Mann-Whitney *U* test. An asterisk (*) indicates a P<0.05, while "ns" denotes no significant difference (P>0.05). PTs, primary tumors; BMs, brain metastases; NSCLC, non-small cell lung cancer.

expression to negative. Overall, TPS grading demonstrated moderate agreement (κ=0.653) (*Figure 2C*).

Discrepancies in TILs between BMs and PTs

The Wilcoxon signed-rank test revealed significant heterogeneity, showing a decrease in the infiltration density of $CD3^+$ T cells (mean 698.8 cells/mm^2 in BMs *vs.* 1,007.5 cells/mm^2 in PTs, P<0.001), $CD8^+$ T cells (mean 406.2 cells/mm^2 in BMs *vs.* 696.5 cells/mm^2 in PTs, P<0.001), $CD20^+$ B cells (mean 163.3 cells/mm^2 in BMs *vs.* 284.7 cells/mm^2 in PTs, P<0.001), and $CD68^+$ macrophages (mean 519.4 cells/mm^2 in BMs *vs.* 623.1 cells/mm^2 in PTs, P=0.02) between paired BMs and PTs. However, the density of $CD4^+$ cells showed no significant change (mean 307.8 cells/mm^2 in BMs *vs.* 399.6 cells/mm^2 in PTs, P=0.10). Among the paired samples, 22 cases (84.6%) exhibited decreased $CD8^+$ T cell density, 23 cases (88.5%) had decreased $CD3^+$ T cell density, 16 cases (61.5%) showed decreased $CD4^+$ T cell density, 22 cases (84.6%) had reduced $CD20^+$ B cell density, and 21 cases (80.8%) showed decreased $CD68^+$ macrophage density in BMs compared to PTs (*Table 2* and *Figure 3A*).

The Mann-Whitney test was also used to evaluate general differences in IC infiltration density between non-paired samples of BMs and PTs. The results showed significantly lower densities of $CD3^+$ T cells (P=0.003), $CD8^+$ T cells (P=0.002), and $CD20^+$ B cells (P=0.02) in BMs compared to PTs. Although the densities of $CD4^+$ T cells (P=0.15) and $CD68^+$ macrophages (P=0.052) were also lower in BMs, these differences were not statistically significant (*Figure 3B*).

TLS presence and count in BMs and PTs

TLS presence and count were evaluated in both PTs and BMs (*Figure 1*). In PTs, TLS were observed in 13 cases (50%), with an average of 6 TLS per case where TLS were present. Among these, 3 cases (11.5%) had early TLS, 10 cases (38.5%) had mature follicle-like TLS. In contrast, TLS were identified in only 4 cases (15.4%) of BMs, with a mean count of 2 TLS per case. Notably, none of the BMs

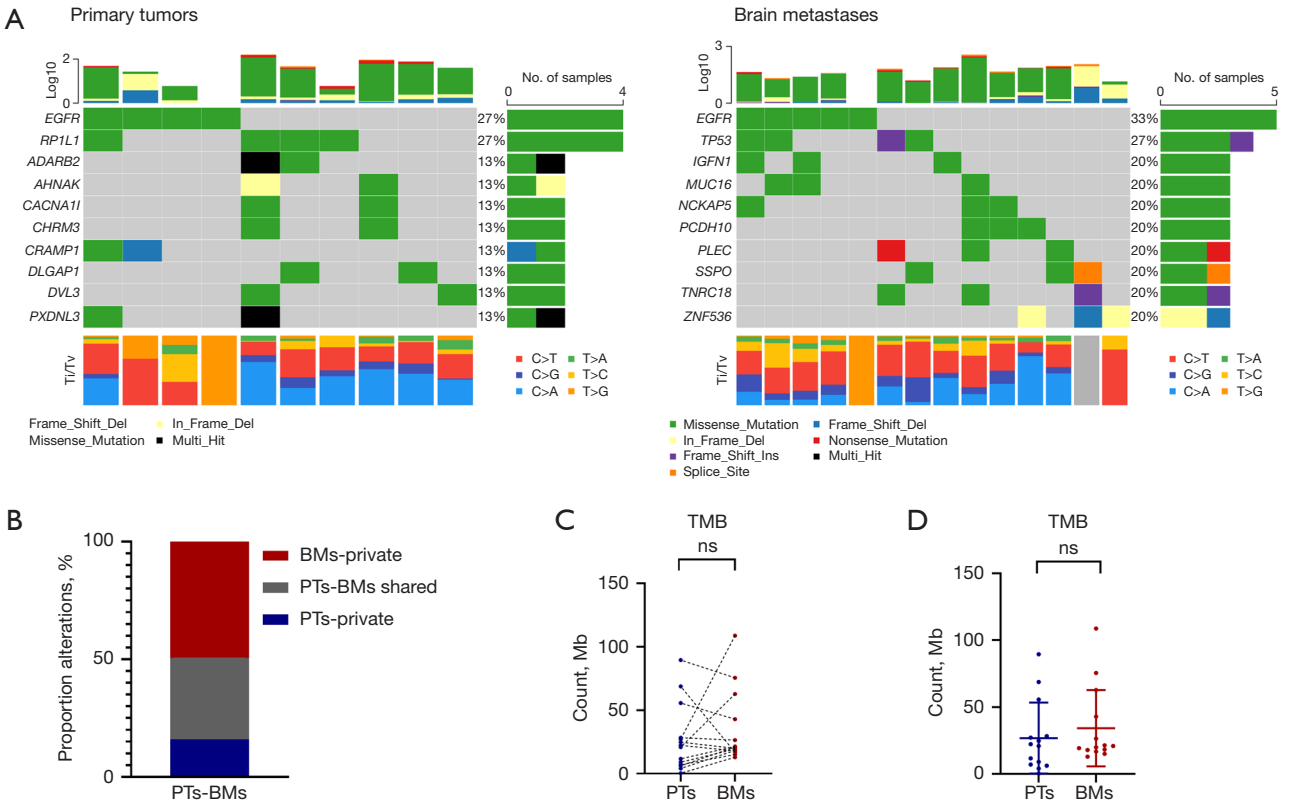

Figure 4 Analysis of mutational features in NSCLC PTs and BMs. (A) Heatmaps displaying mutational features in PTs and BMs; (B) proportion of mutations shared between PTs and BMs; (C) comparison of changes in TMB between paired PTs and BMs, analyzed using the Wilcoxon signed-rank test; (D) differences in TMB between unpaired PTs and BMs, analyzed using the Mann-Whitney *U* test. "ns" denotes no significant difference (P>0.05). Ti/Tv, transitions/transversions; PTs, primary tumors; BMs, brain metastases; NSCLC, non-small cell lung cancer; TMB, tumor mutational burden.

exhibited mature follicle-like TLS with CD21 positive staining. There was a significant reduction in TLS in BMs compared to matched PTs (P=0.03).

Genomic discordances and TMB between BMs and PTs

Among the mutations identified in BMs, only 34.69% were present in the paired PTs. BMs showed an increased frequency of mutations in several genes, including *TP53* (27%), *IGFN1* (20%), *MUC16* (20%), *NCKAP5* (20%), *PCDH10* (20%), *SSPO* (20%), *PLEC* (20%), *TNRC18* (20%), and *ZNF536* (20%). These genes mainly associated in tumor progression and metastasis. Notably, an additional EGFR mutation at exon 21 (L858R) was identified in one BM case (*Figure 4A*,*4B*).

TMB was assessed and compared between PTs and BMs. The mean TMB was slightly higher in BMs than in PTs, but this difference was not statistically significant (mean TMB: 34.2/Mb in BMs *vs.* 26.8/Mb in PTs; P=0.30, Wilcoxon signed-rank test; P=0.45, Mann-Whitney test). Of the cases analyzed, eight exhibited an increased TMB, while six showed a decreased TMB (*Table 2* and *Figure 4C*,*4D*).

Prognostic significance of immune biomarkers in BMs

The relationship between immune biomarkers and OS in BMs was analyzed based on the infiltration density of PD-L1 and TILs, categorized into high (above median) and low subgroups. In BMs, a higher density of $CD20^+$ B cells was significantly associated with improved outcomes (P=0.007), while a high density of $CD8^+$ T cells showed a trend toward better OS (P=0.06) (*Figure 5A*). The presence of TLS in BMs was also associated with a trend toward better OS (P=0.09) (*Figure 5B*). Multivariate analysis, accounting

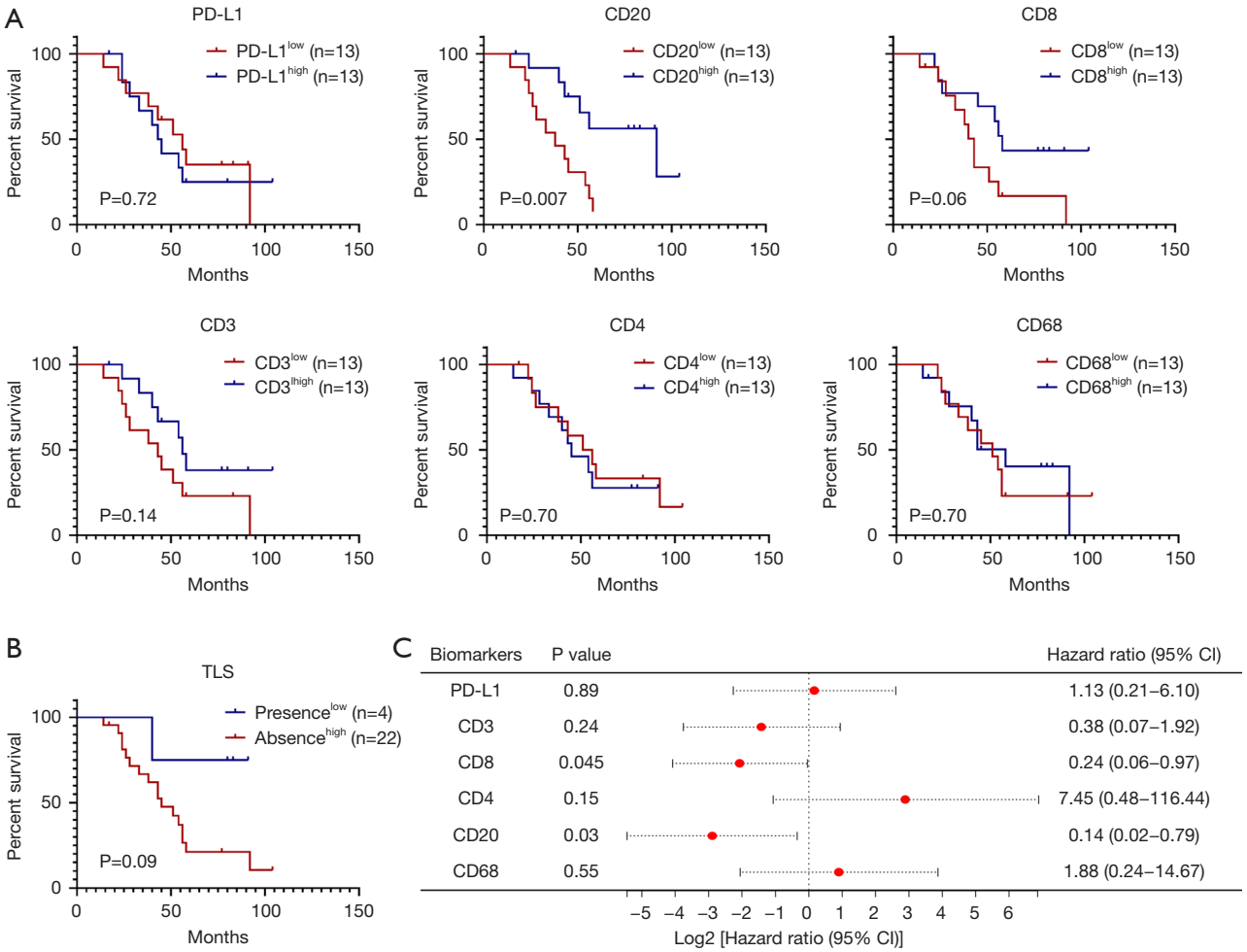

Figure 5 Prognostic analysis related to immune features in BMs of NSCLC. (A) OS associated with the infiltrating density of PD-L1$^+$ cells and immune cells in BMs; (B) OS based on the presence of TLS in BMs; (C) forest plot illustrating the prognostic value of PD-L1 and immune cell density in BMs of NSCLC. PD-L1, programmed death-ligand 1; low, below the median; high, above the median; TLS, tertiary lymphoid structures; CI, confidence interval; BMs, brain metastases; NSCLC, non-small cell lung cancer; OS, overall survival.

for clinicopathological factors such as sex, age, smoking history, and histology, identified high densities of CD8$^+$ T cells [P=0.045; HR =0.24; 95% confdence interval (CI): 0.06–0.97] and CD20$^+$ B cells (P=0.03; HR =0.14; 95% CI: 0.02–0.79) as low-risk factors for cancer-related death in NSCLC with BMs (*Figure 5C*).

Discussion

The heterogenous immune microenvironment impacts the therapeutic response and prognosis of NSCLC patients with BMs. This study explored differences in key immune biomarkers—PD-L1 expression, TILs, TLS, and TMB—by analyzing surgical samples from paired BMs and PTs of NSCLC. Our findings indicate that, compared to primary NSCLC tumors, BMs exhibit an increase in TPS and TMB, alongside a notable decrease in TILs and a loss of mature TLS. These results underscore the potential for heterogeneous responses to immunotherapy in these cases. Furthermore, our study highlights the prognostic relevance of CD20$^+$ B cell infiltration in NSCLC with BMs.

Intertumoral heterogeneity of PD-L1 has been noted in clinical practice. Several studies have reported inconsistencies in PD-L1 expression between metastatic and primary NSCLC tumors (2-4). In NSCLC with matched BMs, Zhou *et al.* found that in a comparative study of 25 BMs cases, 10 cases (40%) exhibited discordant PD-L1 expression (P=0.025) (17). Mansfield *et al.* performed a paired analysis

of 146 BMs, including biopsies from 73 patients, revealing a 14% discrepancy in PD-L1 expression with a κ coefficient of 0.71 (2). A systematic review of six studies on biopsied or resected BMs showed a 19% discordance in TC PD-L1 expression between PTs and BMs (95% CI: 10–27%), with the highest discordance observed in the 1–50% expression category (4). In this study, PD-L1 expression on TCs was generally higher in BMs compared to PTs, with an elevated TPS observed in a greater number of BM cases. Non-paired analysis of PD-L1 further showed that the number of PD-L1$^+$ cells did not significantly increase, suggesting that the reduction in PD-L1$^+$ IC density may be due to the overall decrease in IC infiltration in BMs. These findings suggest that the progression of NSCLC to BM is mainly associated with increased PD-L1 expression in TCs, potentially facilitating immune evasion. From a clinical perspective on immunotherapy cut-offs, moderate agreement in TPS was observed among paired samples, with 76.92% of patients maintaining a consistent TPS grade in clinical assessments, indicating the potential reliability of TPS grading in guiding treatment decisions.

In addition to changes in PD-L1 expression, the immune microenvironment may undergo dynamic alterations during metastasis or treatment (18-20). The microenvironment in BM is generally composed of extracellular matrix, tissue-resident cells and blood-derived ICs (21). The heterogeneity of ICs during recurrence and metastasis is particularly relevant in advanced cancers with multiple metastases and may exhibit organ-specific variations (22-24). Mansfield *et al.* observed reduced lymphocyte infiltration in BMs compared to PTs (2). Similarly, Kudo *et al.* BMs exhibited lower T cell and elevated macrophage infiltration compared with PTs (25). Our study revealed significant changes in several IC subsets in BMs, including marked reductions in CD3$^+$ T cells, CD8$^+$ effector T cells, CD20$^+$ B cells, and CD68$^+$ macrophages compared to PTs. In non-paired studies, it was similarly found that lymphocyte infiltration in BMs is generally lower than that in primary lung tumors, indicating a weaker capacity for lymphocyte recruitment in non-NSCLC during BM.

TLS play a critical role in facilitating IC interactions and enhancing anti-tumor immunity (6). Our study identified a loss of TLS in BMs compared to PTs, notably an absence of mature TLS in BMs. This suggests a reduced ability to recruit ICs to the tumor site and a deficiency in organized immune responses. A recent study on TLS in 17 cases of lung cancer with BMs also reported a decrease in TLS density and an immature status compared to PTs (26). Their absence and immature status in BMs may hinder IC activation and function, exacerbating the immunosuppressive environment. The absence and immaturity of TLS in BMs may impair IC activation and function, thereby exacerbating the immunosuppressive environment. This may explain why lung adenocarcinoma patients with BMs have been reported to have inferior responses to ICI-based treatments, with lower disease control rates and shorter progression-free survival (PFS) (27). These findings underscore the importance of promoting TLS formation and enhancing TIL migration and infiltration in BMs as part of immunotherapy strategies.

Moreover, we showed the correlations between TILs density and prognosis in BMs. Higher lymphocyte density was generally associated with better outcomes in BMs. Camy *et al.* similarly reported that a higher density of CD8$^+$ T cells in BMs was marginally linked to improved prognosis (28). Regarding TLS, Nohira *et al.* observed a significant correlation between TLS density and enhanced postoperative survival (26). Our study also noted a trend towards a correlation between the presence of TLS and OS, approaching statistical significance, possibly due to the limited number of cases. Additionally, our study highlighted the significant prognostic value of CD20$^+$ B cells in BMs. B cells, which are predominantly associated with TLS, facilitate the recruitment of various ICs, such as T cells, natural killer (NK) cells, and dendritic cells, and enhancing antigen presentation to T cells (6,29,30). In metastatic melanoma, B cell-related genes have been found to be enriched in tissues from patients responding to immune checkpoint blockade therapy (31). Further investigation into the role of CD20$^+$ B cells in NSCLC with BMs is warranted.

At the genomic level, we investigated discrepancies in gene mutations and TMB between PTs and BMs. Consistent with a previous study showing an overall concordance of 45.6% in gene mutations between PTs and metastases (32), our findings revealed that only 34.69% of mutations were shared between paired PTs and BMs in NSCLC. Notably, there was a significant increase in TP53 and MUC16 mutations in BMs, which have been reported to be associated with TMB (33-35). This suggests that genomic discordance and alterations in non-synonymous mutations may occur during NSCLC metastasis. Although discrepancies in TMB between PTs and matched BMs have not been extensively reported, our study found a general increase in the number of non-synonymous mutations and TMB in some BMs. These results underscore potential variations in mutation profiles within BMs, which may contribute to the heterogeneity of

the immune microenvironment in NSCLC with BMs.

One of the strengths of this study lies in its utilization of surgical samples and digital image analysis, which minimizes variability in biopsy procedures and pathologist interpretations. This approach enhances the accuracy of quantifying PD-L1 expression and TILs populations. However, the study has limitations. The sample size is relatively small due to the rarity of paired surgical tissue samples. Additionally, WES and TMB testing were conducted only on recent paired samples collected within the last few years. Given the diverse subtypes of tumor-associated ICs, this study focused primarily on a few of the most common types through digital image quantification analysis. Despite these limitations, the study provides valuable insights for future research on which types of ICs to prioritize in the context of BMs from NSCLC, as well as for subsequent investigations into the immune microenvironment.

Conclusions

Our study highlights the immunological features of BMs in NSCLC, revealing an increase in the TPS of PD-L1 expression and TMB, but a reduced presence of TILs, a loss of mature TLS in matched BMs compared to PTs. A high density of $CD20^+$ B cells may serve as a potential biomarker for NSCLC with BMs. Further investigation into the heterogeneity of the immune microenvironment and its impact on immune responses will be valuable for addressing the varied responses to immunotherapy and guiding treatment strategies for NSCLC patients with BMs.

Acknowledgments

Funding: This work is supported by the National Natural Science Foundation of China (No. 82003155 to J.W.), and the Tianjin Key Medical Discipline (Pathology) Construction Project (No. TJYXZDXK-012A to Y.Z.).

Footnote

Reporting Checklist: The authors have completed the STROBE reporting checklist. Available at https://tlcr.amegroups.com/article/view/10.21037/tlcr-24-735/rc

Data Sharing Statement: Available at https://tlcr.amegroups.com/article/view/10.21037/tlcr-24-735/dss

Peer Review File: Available at https://tlcr.amegroups.com/article/view/10.21037/tlcr-24-735/prf

Conflicts of Interest: All authors have completed the ICMJE uniform disclosure form (available at https://tlcr.amegroups.com/article/view/10.21037/tlcr-24-735/coif). Y.Z. received funding from Tianjin Key Medical Discipline (Pathology) Construction Project (No. TJYXZDXK-012A) to this study. J.W. received funding from National Natural Science Foundation of China (No. 82003155) to this study. The other authors have no conflicts of interest to declare.

Ethical Statement: The authors are accountable for all aspects of the work in ensuring that questions related to the accuracy or integrity of any part of the work are appropriately investigated and resolved. The study was conducted in accordance with the Declaration of Helsinki (as revised in 2013) and was approved by the Ethics Committee of the Tianjin Medical University Cancer Institute and Hospital (No. bc20241476). Written informed consent was waived due to the retrospective nature of this study.

References

1. Wang Q, Fang Y, Li C, et al. Differential organ-specific tumor response to first-line immune checkpoint inhibitor therapy in non-small cell lung cancer-a retrospective cohort study. Transl Lung Cancer Res 2023;12:312-21.
2. Mansfield AS, Aubry MC, Moser JC, et al. Temporal and spatial discordance of programmed cell death-ligand 1 expression and lymphocyte tumor infiltration between paired primary lesions and brain metastases in lung cancer. Ann Oncol 2016;27:1953-8.
3. Wu J, Sun W, Yang X, et al. Heterogeneity of programmed death-ligand 1 expression and infiltrating lymphocytes in paired resected primary and metastatic non-small cell lung cancer. Mod Pathol 2022;35:218-27.
4. Tonse R, Rubens M, Appel H, et al. Systematic review and meta-analysis of PD-L1 expression discordance

between primary tumor and lung cancer brain metastasis. Neurooncol Adv 2021;3:vdab166.
5. Hendry S, Salgado R, Gevaert T, et al. Assessing Tumor-Infiltrating Lymphocytes in Solid Tumors: A Practical Review for Pathologists and Proposal for a Standardized Method from the International Immuno-Oncology Biomarkers Working Group: Part 2: TILs in Melanoma, Gastrointestinal Tract Carcinomas, Non-Small Cell Lung Carcinoma and Mesothelioma, Endometrial and Ovarian Carcinomas, Squamous Cell Carcinoma of the Head and Neck, Genitourinary Carcinomas, and Primary Brain Tumors. Adv Anat Pathol 2017;24:311-35.
6. Helmink BA, Reddy SM, Gao J, et al. B cells and tertiary lymphoid structures promote immunotherapy response. Nature 2020;577:549-55.
7. de Visser KE, Joyce JA. The evolving tumor microenvironment: From cancer initiation to metastatic outgrowth. Cancer Cell 2023;41:374-403.
8. Büttner R, Longshore JW, López-Ríos F, et al. Implementing TMB measurement in clinical practice: considerations on assay requirements. ESMO Open 2019;4:e000442.
9. Yarchoan M, Hopkins A, Jaffee EM. Tumor Mutational Burden and Response Rate to PD-1 Inhibition. N Engl J Med 2017;377:2500-1.
10. Devarakonda S, Rotolo F, Tsao MS, et al. Tumor Mutation Burden as a Biomarker in Resected Non-Small-Cell Lung Cancer. J Clin Oncol 2018;36:2995-3006.
11. Singal G, Miller PG, Agarwala V, et al. Association of Patient Characteristics and Tumor Genomics With Clinical Outcomes Among Patients With Non-Small Cell Lung Cancer Using a Clinicogenomic Database. JAMA 2019;321:1391-9.
12. Bankhead P, Loughrey MB, Fernández JA, et al. QuPath: Open source software for digital pathology image analysis. Sci Rep 2017;7:16878.
13. Posch F, Silina K, Leibl S, et al. Maturation of tertiary lymphoid structures and recurrence of stage II and III colorectal cancer. Oncoimmunology 2018;7:e1378844.
14. Ren F, Xie M, Gao J, et al. Tertiary lymphoid structures in lung adenocarcinoma: characteristics and related factors. Cancer Med 2022;11:2969-77.
15. Saunders CT, Wong WS, Swamy S, et al. Strelka: accurate somatic small-variant calling from sequenced tumor-normal sample pairs. Bioinformatics 2012;28:1811-7.
16. Wang K, Li M, Hakonarson H. ANNOVAR: functional annotation of genetic variants from high-throughput sequencing data. Nucleic Acids Res 2010;38:e164.
17. Zhou J, Gong Z, Jia Q, et al. Programmed death ligand 1 expression and CD8(+) tumor-infiltrating lymphocyte density differences between paired primary and brain metastatic lesions in non-small cell lung cancer. Biochem Biophys Res Commun 2018;498:751-7.
18. Sang J, Liu P, Wang M, et al. Dynamic Changes in the Immune Microenvironment in Tumor-Draining Lymph Nodes of a Lewis Lung Cancer Mouse Model After Microwave Ablation. J Inflamm Res 2024;17:4175-86.
19. Cho H, Kim JE, Hong YS, et al. Comprehensive evaluation of the tumor immune microenvironment and its dynamic changes in patients with locally advanced rectal cancer treated with preoperative chemoradiotherapy: From the phase II ADORE study. Oncoimmunology 2022;11:2148374.
20. Wu J, Sun W, Zhang Y, et al. Impact of platinum-based chemotherapy on the tumor mutational burden and immune microenvironment in non-small cell lung cancer with postoperative recurrence. Clin Transl Oncol 2024;26:1738-47.
21. Wang Y, Chen R, Wa Y, et al. Tumor Immune Microenvironment and Immunotherapy in Brain Metastasis From Non-Small Cell Lung Cancer. Front Immunol 2022;13:829451.
22. Jiménez-Sánchez A, Memon D, Pourpe S, et al. Heterogeneous Tumor-Immune Microenvironments among Differentially Growing Metastases in an Ovarian Cancer Patient. Cell 2017;170:927-938.e20.
23. Van den Eynde M, Mlecnik B, Bindea G, et al. The Link between the Multiverse of Immune Microenvironments in Metastases and the Survival of Colorectal Cancer Patients. Cancer Cell 2018;34:1012-1026.e3.
24. Restle D, Dux J, Li X, et al. Organ-specific heterogeneity in tumor-infiltrating immune cells and cancer antigen expression in primary and autologous metastatic lung adenocarcinoma. J Immunother Cancer 2023;11:e006609.
25. Kudo Y, Haymaker C, Zhang J, et al. Suppressed immune microenvironment and repertoire in brain metastases from patients with resected non-small-cell lung cancer. Ann Oncol 2019;30:1521-30.
26. Nohira S, Kuramitsu S, Ohno M, et al. Tertiary Lymphoid Structures in Brain Metastases of Lung Cancer: Prognostic Significance and Correlation With Clinical Outcomes. Anticancer Res 2024;44:3615-21.
27. Zhou J, Wu Y, Xie M, et al. The clinical outcome and risk factors analysis of immune checkpoint inhibitor-based treatment in lung adenocarcinoma patients with brain metastases. Transl Lung Cancer Res 2022;11:656-69.

28. Camy F, Karpathiou G, Dumollard JM, et al. Brain metastasis PD-L1 and CD8 expression is dependent on primary tumor type and its PD-L1 and CD8 status. J Immunother Cancer 2020;8:e000597.
29. Laumont CM, Banville AC, Gilardi M, et al. Tumour-infiltrating B cells: immunological mechanisms, clinical impact and therapeutic opportunities. Nat Rev Cancer 2022;22:414-30.
30. Fridman WH, Meylan M, Petitprez F, et al. B cells and tertiary lymphoid structures as determinants of tumour immune contexture and clinical outcome. Nat Rev Clin Oncol 2022;19:441-57.
31. Cabrita R, Lauss M, Sanna A, et al. Tertiary lymphoid structures improve immunotherapy and survival in melanoma. Nature 2020;577:561-5.
32. Tang WF, Wu M, Bao H, et al. Timing and Origins of Local and Distant Metastases in Lung Cancer. J Thorac Oncol 2021;16:1136-48.
33. Hu C, Zhao L, Liu W, et al. Genomic profiles and their associations with TMB, PD-L1 expression, and immune cell infiltration landscapes in synchronous multiple primary lung cancers. J Immunother Cancer 2021;9:e003773.
34. Li X, Pasche B, Zhang W, et al. Association of MUC16 Mutation With Tumor Mutation Load and Outcomes in Patients With Gastric Cancer. JAMA Oncol 2018;4:1691-8.
35. Zhang F, Li X, Chen H, et al. Mutation of MUC16 Is Associated With Tumor Mutational Burden and Lymph Node Metastasis in Patients With Gastric Cancer. Front Med (Lausanne) 2022;9:836892.

Cite this article as: Zhang Y, Cheng R, Ding T, Wu J. Discrepancies in PD-L1 expression, lymphocyte infiltration, and tumor mutational burden in non-small cell lung cancer and matched brain metastases. Transl Lung Cancer Res 2024;13(12):3590-3602. doi: 10.21037/tlcr-24-735